

Periodic and chaotic dynamics of a sliding driven oscillator with dry friction

F. Bellido*, J.B. Ramírez-Malo

Dpto. de Física de la Materia Condensada, Facultad de Ciencias, Universidad de Cádiz, Campus del Río San Pedro, 11510 Puerto Real (Cádiz), Spain

Received 20 January 2005; received in revised form 14 April 2006; accepted 8 May 2006

Abstract

We have performed a numerical study of the dynamics of a harmonically forced sliding oscillator with two degrees of freedom and dry friction. The study of the four-dimensional dynamical system corresponding to the two non-linear motion equations can be reduced, in this case, to the study of a three-dimensional Poincaré map. The behaviour of the system has been investigated calculating bifurcation diagrams, time series, periodic and chaotic attractors and basins of attraction. Furthermore, a systematic study of the stability of periodic solutions and their bifurcations has been carried out applying the Floquet theory. The results show rich dynamics being very sensitive to the changes in forcing amplitudes (control parameter), where periodic and chaotic states alternatively appear. It is shown how the system exhibits different types of bifurcational phenomena (saddle-node, symmetry-breaking, period-doubling cascades and intermittent transitions to chaos) into relatively narrow intervals of the control parameter. Moreover, a collection of chaotic attractors was computed to show the evolution of the chaotic regime. Finally, basins of attraction were calculated. In all the cases studied, the basins exhibit fractal structure boundaries and, when more of two attractors are coexisting, we have found *Wada basin boundaries*.

© 2006 Elsevier Ltd. All rights reserved.

Keywords: Dry friction; Bifurcations; Floquet multipliers; Chaotic attractors; Basins of attraction; Wada basin boundaries

1. Introduction

The vibrational behaviour of mechanical systems with dry friction play an important role both in problems of mechanical engineering as well as from a theoretical viewpoint. From the point of view of practical applications, many mechanical devices governed by non-linear motion equations may exhibit, under certain conditions, irregular changes in their motion (jumps, multi-periodicity, etc.) [1]. Hence, the study of governing equations is of considerable practical value for designing and controlling these devices. On the other hand, the non-linearities of systems with dry friction are responsible for different types of periodic, chaotic and bifurcational behaviours. Thus, these systems may provide mathematical models with rich dynamics enabling the application of non-linear dynamical systems and chaos theory.

Many studies have been carried out on systems whose dynamics include alternating static and kinetic states. They have mainly focused on the *stick-slip* phenomenon [2], where

the non-linearities enter in the motion equations by using piecewise-smooth functions for the modelling of static and dynamic friction forces [3]. When the mechanical systems are permanently sliding, the dynamical friction forces generally depend on the relative velocity of the bodies in contact by means of the relationship $\mathbf{F}_r = -(\mathbf{v}_r/v_r)f(v_r)$ [1], where \mathbf{F}_r is the dynamical friction force, \mathbf{v}_r is the relative velocity and $f(v_r)$ is a smooth function, which includes the normal load and the kinetic friction coefficient $\mu_d = \mu_d(v_r)$. In this case, the non-linear motion equations constitute a smooth vector field, where different kinetic friction dependent velocity models [4–7] can be used. Thus, bifurcation theory for smooth system, as well as the classical Floquet theory, can be applied to study the behaviour and the stability of steady-state response of these systems.

In this work, we present a numerical study of a sliding driven rigid body with two degrees of freedom, which has one point of contact with a surface on which a dynamic dry friction force is acting. The system exhibits oscillations in the perpendicular direction to the slide (*transversal oscillations*) and it is periodically forced in the direction in which it is sliding. This system may be considered as a first very simple model of a

* Corresponding author.

E-mail address: francisco.bellido@uca.es (F. Bellido).

sliding articulated trailer subjected to a harmonic traction. Also, it may constitute a model of small sliding devices in mechanical machines. On the hypothesis that systems with these characteristics exhibit instabilities in the periodic oscillations and chaotic dynamics, which can produce loss of control in articulated vehicles or bad operations of these devices, the study of the dynamics of this simple model can contribute to the understanding of certain behaviours, which should be avoided in real mechanical systems.

2. Mechanical system, motion equations and stability of periodic solutions

The mechanical system studied consists of a rectangular-section rod of mass M and length L oscillating into an horizontal plane (Fig. 1). The movement of the origin point O'' of the $X''Y''Z''$ internal framework, fixed to one end of the rod, is restricted to a straight line parallel to the X -axis. The other end of the rod is supported by a conveyor belt through a small needle, while the belt and the $O'X'Y'Z'$ frame fixed to it are moving horizontally with a constant speed (v_b). Under these conditions the system carries out a two-dimensional sliding motion with dry friction between the trip needle (point S) and the belt surface. Finally, an external device is producing a periodic force given by $F = B \cos(\omega t)$, which is driving the system in X direction.

The geometrical characteristics of the system allow the use of variables x and θ as appropriated generalized coordinates to formulate the dynamical problem. As it is shown in Fig. 1, x indicates the position of point O'' in a fixed framework $OXYZ$ and θ is the angular displacement of the rod. The equations of motion of the system were calculated using the well-known Lagrange's equations

$$\frac{d}{dt} \frac{\partial T}{\partial \dot{q}_i} - \frac{\partial T}{\partial q_i} = Q_{q_i}, \quad q_1 = x, \quad q_2 = \theta, \tag{1}$$

where

$$T = \frac{1}{2}M(\dot{x} - v_b)^2 + \frac{1}{2}I\dot{\theta}^2 - \frac{1}{2}ML\dot{\theta}(\dot{x} - v_b) \sin \theta \tag{2}$$

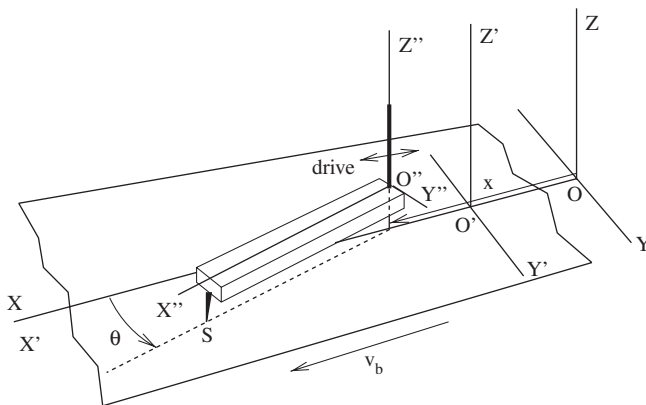


Fig. 1. Sketch of the mechanical system.

is the kinetic energy of the rod (I is the moment of inertia of the rod with respect to the Z'' -axis), and Q_x and Q_θ are the generalized forces associated with x and θ coordinates, respectively.

In this problem, the generalized forced can be expressed in the form

$$Q_x = B \cos(\omega t) - \frac{1}{v_{rel.}}(\dot{x} - v_b - \dot{\theta}L \sin \theta)F_r, \tag{3}$$

$$Q_\theta = \frac{1}{v_{rel.}}[(\dot{x} - v_b) \sin \theta - \dot{\theta}L]LF_r, \tag{4}$$

where

$$v_{rel.} = \sqrt{(\dot{x} - v_b - \dot{\theta}L \sin \theta)^2 + (\dot{\theta}L \cos \theta)^2} \tag{5}$$

is the modulus of the relative speed between the contact point S and the belt.

The term F_r in Eqs. (3) and (4) is the modulus of the dry friction force applied in the point S by the belt. Assuming that the mechanical behaviour of the system is determined by the driven sliding, a friction force model characterized by a linear dependence [5] of the relative speed will be used. Thus, considering the classical dry friction law $F_r = \mu_k N$, where N is the magnitude of the force acting in the normal direction on the sliding point S , the dynamic friction coefficient takes the following form [6]:

$$\mu_k(v_{rel.}) = \mu_k^0 + \eta v_{rel.}, \quad \mu_k^0 > 0, \quad \eta > 0. \tag{6}$$

According to the above scheme, the motion equations are

$$\ddot{x} = \frac{1}{c_1 - c_2^2 \sin^2 \theta} [c_2(I\dot{\theta}^2 \cos \theta + Q_\theta \sin \theta) + IQ_x], \tag{7a}$$

$$\ddot{\theta} = \frac{1}{c_1 - c_2^2 \sin^2 \theta} (c_2^2 \dot{\theta}^2 \sin \theta \cos \theta + c_2 Q_x \sin \theta + MQ_\theta), \tag{7b}$$

where $c_1 = MI$ and $c_2 = \frac{1}{2}ML$.

Using non-dimensional normalized time $\tau = \omega t$ and the coordinates

$$x_0 = \frac{x}{L}, \quad x_1 = \dot{x}, \quad x_2 = \theta, \quad x_3 = \dot{\theta}, \tag{8}$$

a second-order differential equations system (7a)–(7b) can be written in the following non-dimensional dynamical system form:

$$\dot{x}_0 = x_1, \tag{9a}$$

$$\dot{x}_1 = \frac{1}{\omega^2(c_1 - c_2^2 \sin^2 x_2)L} [c_2(I\omega^2 x_3^2 \cos x_2 + Q'_{x_2} \sin x_2) + IQ'_{x_0}], \tag{9b}$$

$$\dot{x}_2 = x_3, \tag{9c}$$

$$\dot{x}_3 = \frac{1}{\omega^2(c_1 - c_2^2 \sin^2 x_2)} (c_2^2 \omega^2 x_3^2 \sin x_2 \cos x_2 + c_2 Q'_{x_0} \sin x_2 + MQ'_{x_2}), \tag{9d}$$

where

$$Q'_{x_0} = -(\omega x_1 - v_b - \omega x_3 L \sin x_2) N \left(\frac{\mu_k^0}{v'_{rel.}} + \eta \right) + B \sin \tau, \tag{10a}$$

$$Q'_{x_2} = -(\omega x_1 - v_b - \omega x_3 L) N \left(\frac{\mu_k^0}{v'_{rel.}} + \eta \right) L, \tag{10b}$$

$$\left(v'_{rel.} = \sqrt{(\omega x_1 - v_b - \omega x_3 L \sin x_2)^2 + (\omega x_3 L \cos x_2)^2} \right)$$

are the generalized forces using non-dimensional time τ .

It is firstly noted that the coordinate x_0 does not appear in the equations of motion of the mechanical system. Thus, the dynamical system given by Eqs. (9a)–(9d) can be studied considering, on one hand, the three-dimensional dynamical system given by Eqs. (9b)–(9d), and, on the other hand, Eq. (9a), which can be integrated once the $x_1(\tau)$ function is known.

The system of equations (9b)–(9d) constitutes a non-autonomous system, which can be written concisely in the form

$$\dot{\mathbf{x}} = \mathbf{F}(\mathbf{x}, t; \mathbf{s}), \tag{11}$$

where $\mathbf{x} \equiv (x_1, x_2, x_3)$ is the state vector, $\mathbf{s} \equiv (M, L, v_b, \mu_k^0, \eta, B, \omega)$ is a parameter vector and $\mathbf{F} \equiv (F_1, F_2, F_3)$ is the periodic vector field formed by the functions of the right-hand side of Eqs. (9b)–(9d). Once the parameter values $\mathbf{s} = \mathbf{s}_0$ and a set of initial conditions $(t_0, x_{10}, x_{20}, x_{30})$ are fixed, it is possible to associate the map $f : \mathbb{R}^3 \rightarrow \mathbb{R}^3$ to the solution of the dynamical system. The discrete sequence of points $\mathbf{x}_n = f^n(\mathbf{x}_0)$ ($n = 1, 2, 3, \dots$; $\mathbf{x}_0 \equiv (x_{10}, x_{20}, x_{30})$), where f^n means n -times iterated f map, can be obtained by sampling the orbit points at time $\tau = \tau_0 + n\Delta\tau$. Taking $\Delta\tau = T_0$, where T_0 is the external driving period ($T_0 = 2\pi$ in our case), the points of f map are Poincaré sections of the solutions in τ, x_1, x_2, x_3 space [8]. Thus, after discarding the first iterations corresponding to the transient solution of the non-autonomous system, a steady state with period $T_k = kT_0$ (k -period solution, being k an integer) can be represented by k points in \mathbb{R}^3 . If one s_i parameter of \mathbf{s} vector is varied and the dynamical system is integrated for each s_i value, the periodic and chaotic behaviour of the system can be studied by means of the evolution of \mathbf{x}_n Poincaré section into $BP = \{(s_i, \mathbf{x}) \in \mathbb{R}^1 \times \mathbb{R}^3\}$ space.

To study the stability of k -period solutions, the $P = f^k$ Poincaré map was considered. Then, on iteration of a point \mathbf{x}_n on orbit under this map, it is obtained as

$$\mathbf{x}_n = P(\mathbf{x}_n). \tag{12}$$

Thus, k -period solutions of (12) correspond to the fixed points of P map, and the stability analysis of these solutions can be carried out by that of the corresponding fixed points.

As it is known [9], the stability of the fixed points of the P map is determined by the examination of the eigenvalues of the $D_{\mathbf{x}}P|_{\mathbf{x}=\mathbf{x}_n}$ Jacobian matrix of P . To calculate this matrix, a scheme based on Floquet Theory [9,10] is assumed. In this

framework, the Jacobian matrix at \mathbf{x}_n coincides with the monodromy matrix of k -period orbit, which is denoted as

$$M(\tau_k) = D_{\mathbf{x}}P|_{\mathbf{x}=\mathbf{x}_n}, \tag{13}$$

satisfying $M(\tau)$ the so-called variational equation

$$\dot{M}(\tau) = A(\tau)M(\tau) \tag{14}$$

with the initial condition $M(\tau_0) = \mathbf{I}$ (identity matrix). $A(\tau)$ is the Jacobian matrix of vector field, which can be written as

$$A(\tau) = \begin{pmatrix} \frac{\partial F_1}{\partial x_1} & \frac{\partial F_1}{\partial x_2} & \frac{\partial F_1}{\partial x_3} \\ \frac{\partial F_2}{\partial x_1} & \frac{\partial F_2}{\partial x_2} & \frac{\partial F_2}{\partial x_3} \\ \frac{\partial F_3}{\partial x_1} & \frac{\partial F_3}{\partial x_2} & \frac{\partial F_3}{\partial x_3} \end{pmatrix}, \tag{15}$$

where the partial derivatives can be calculated from Eqs. (9b)–(9d).

Integrating numerically the differential equation system (14) from $\tau = \tau_0$ to $\tau = \tau_0 + T_k$, with the initial condition $M(\tau_0) = \mathbf{I}$, the matrix $M(\tau_k = \tau_0 + T_k)$ is obtained. Eigenvalues (Floquet multipliers) λ_i ($i = 1, 2, 3$) of this matrix provide information on the stability of the periodic solutions. Furthermore, when the system evolves into the BP space, the evolution of Floquet multipliers to abandon the unit circle of the complex plane allows for the classification of different types [11] of bifurcations.

3. Numerical simulations and bifurcation diagrams

The dynamics of the system was studied using the following parameter vector: $\mathbf{s} \equiv (M = 1 \text{ kg}, L = 0.25 \text{ m}, v_b = 0.01 \text{ m s}^{-1}, \mu_k^0 = 0.1, \eta = 0.1 \text{ kg s}^{-1}, B, \omega = 1 \text{ s}^{-1})$, where the forcing amplitude B was the parameter to be varied (control parameter). Taking into account the μ_k^0 and η values chosen, it is assumed that a weak dry friction was acting on the mechanical system. Additionally, in our study the problem was focused at relatively low forcing amplitudes. Thus, the control parameter was varied into $B \in [0, 15]N$ interval.

To obtain a preliminary illustration of the behaviour of the system in the forcing range considered, the dynamical system was integrated using a fourth-order Runge–Kutta algorithm over grids of initial conditions for different values of the control parameter. In this way, a collection of steady solutions was determined. Next, starting from a fixed value of the control parameter ($B = 0.4$, for instance), which belongs to an interval where the dynamical system exhibit a very rich dynamics, different trajectories into BP space were computed by slowly increasing and decreasing the B parameter. To ensure that steady solutions are obtained, sufficiently long transients were neglected for each B value considered.

Figs. 2 shows a survey of periodic and chaotic solutions in bifurcation diagrams obtained by the projection of four-dimensional trajectories onto B – x_2 (Fig. 2(a)) and B – x_3 (Fig. 2(b)) planes, (in the first case, the values of the angular variable x_2 have been reduced to the $[-\pi, \pi]$ interval). It may be observed that the general dynamics of the system is characterized by the existence of periodic and chaotic attractors, which alternatively appear into consecutive intervals of forcing

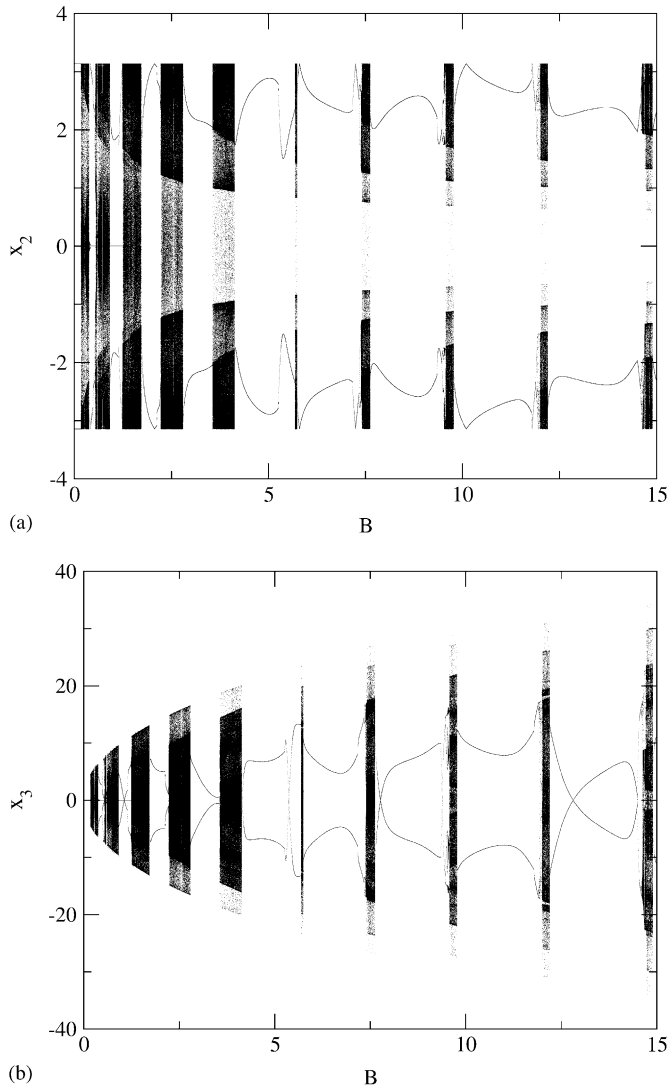


Fig. 2. Overview of Poincaré section bifurcation diagrams, where periodic and chaotic bands alternatively appear: (a) x_2 - B and (b) x_3 - B projections.

amplitudes. As B increases, the width of the intervals where the periodic solutions lie increases. At the same time, the chaotic behaviour suffers an evolution characterized by the tendency of the chaotic attractors to be centred on $x_2 = \pi$ value, instead of being spread into the $[-\pi, \pi]$ interval. Moreover, typically small periodic windows can be found inside the chaos bands. By carefully examining the intervals where the solutions are periodic, abundant bifurcational scenarios, such as saddle-node bifurcations, intermittent transitions to chaos, symmetry-breaking bifurcations and period-doubling cascades, were detected. Symmetry-breaking bifurcations are typical in forced dynamical systems where one or more variables (named x) are invariant under $(x \rightarrow -x, \dot{x} \rightarrow -\dot{x}, t \rightarrow t + \pi/\omega)$ transformation.

To determine the stability of motion, the evolution of periodic attractors was studied in terms of the variation of Floquet multipliers, when the control parameter was varied. The local bifurcations, where solutions lose the stability, were characterized by simultaneously integrating the dynamical system and

the nine differential equations contained in the variational matrix equation (14). For each B value, at the beginning of integration of the last T_k -period cycle, after $\tau = NT_k$ (N integer) simulated time has passed, the initial condition $M(\tau) = \mathbf{I}$ was imposed to the differential equations system. Thus, to finish the integration period, at $\tau + T_k$, the monodromy matrix $M(\tau + T_k)$ of the orbit was obtained (also the Poincaré section). Finally, by using a Raphson–Newton algorithm, the λ_i ($i = 1, 2, 3$) Floquet multipliers were calculated solving the characteristic equation $\det[M(\tau_0 + T_k) - \lambda \mathbf{I}] = 0$.

4. Periodic behaviour. Stability and symmetries

An analysis of the successive periodic intervals in bifurcation diagrams permits to detect various types of periodic behaviour, which evolve in different ways when the control parameter is changed. To organize the description of the different dynamics of the system we will distinguish between low forcing amplitudes ($B \lesssim 0.55$) and mean-large forcing amplitudes ($0.85 \lesssim B \lesssim 15$).

4.1. Low forcing amplitudes

At low B value the system exhibits a varied periodic and bifurcational behaviour mainly based on the coexistence of solutions from $B \approx 0.36$ to $B \approx 0.55$ (Fig. 3). Thus, at $B = 0.4$, the bifurcation diagram shows eight branches corresponding to six coexisting solutions. Two of them are associated to $x_1 = x_1(\tau)$, $x_2 = 0$, $x_3 = 0$ and $x_1 = x_1(\tau)$, $x_2 = \pi$, $x_3 = 0$ solutions, when

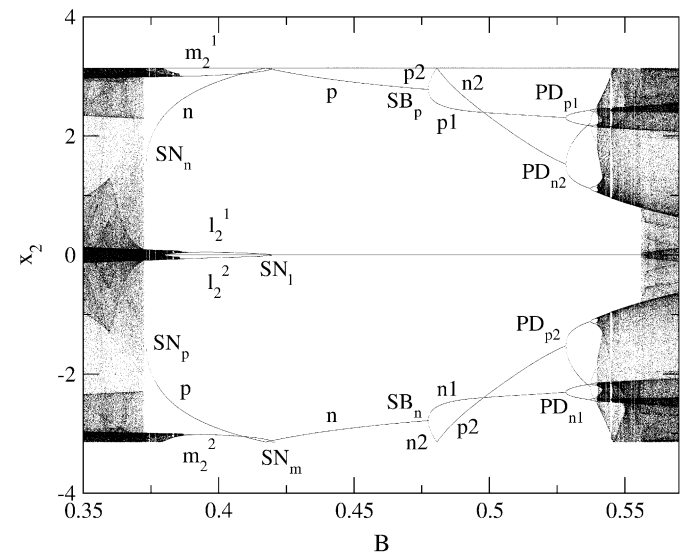


Fig. 3. Bifurcation diagram showing the evolution of the two period-1 n and p mutually symmetric solutions, and the two period-2 l_2^i, m_2^i ($i = 1, 2$) solutions. Period-1 orbits are originated in both SN_n and SN_p saddle-node bifurcations, pass through symmetry-breaking bifurcations (SB_n and SB_p) and, finally, both orbit pairs ($n1, n2$) and ($p1, p2$) created after BS bifurcations undergo period doubling bifurcations (PD) and cascades to chaos. The two period-2 orbits evolve from chaos and are destroyed in both SN_l, SN_m saddle-node bifurcations.

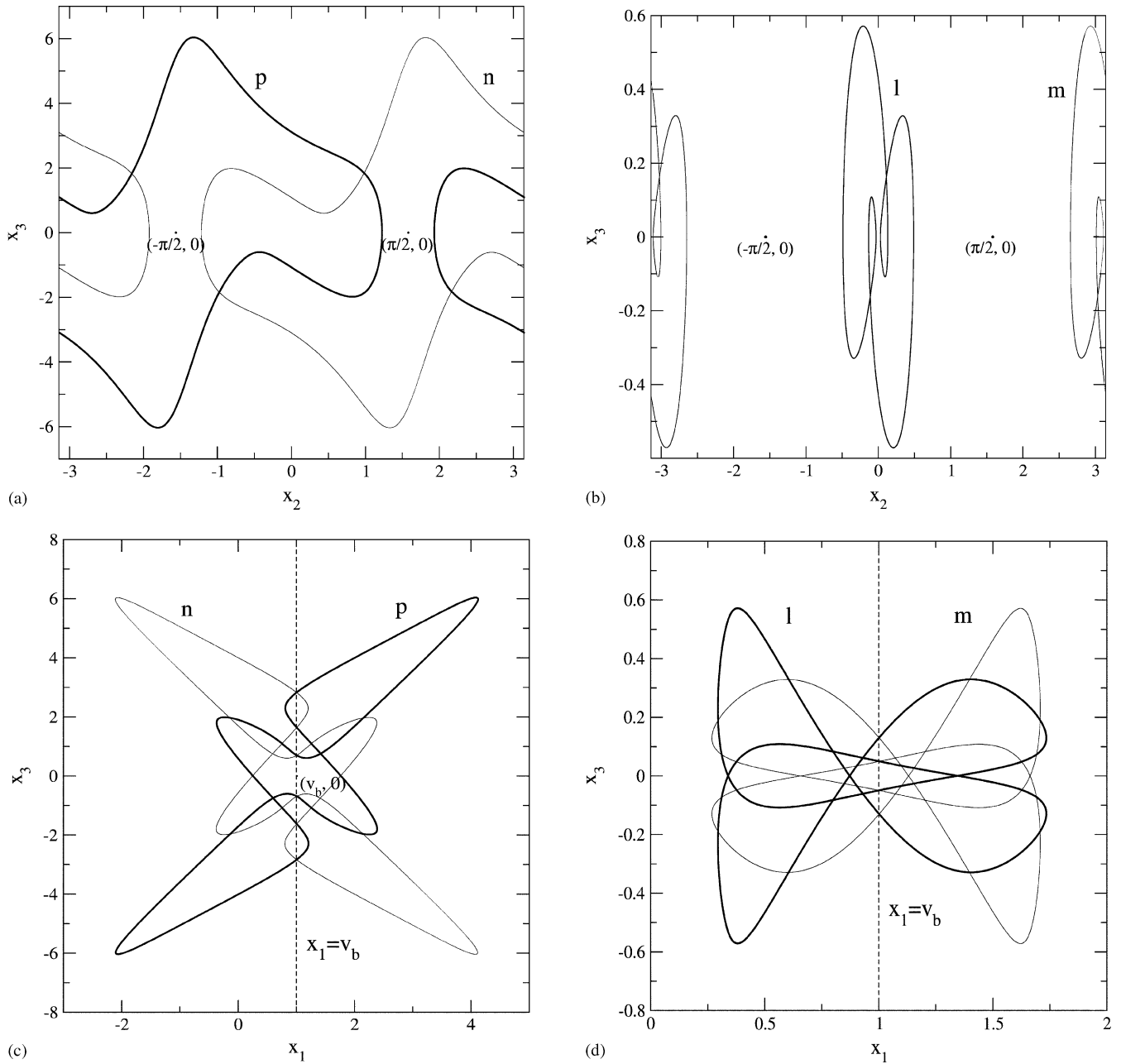


Fig. 4. Projections of the trajectories of coexisting solutions at $B = 0.4$ showing: (a) and (b) the symmetry with respect to the origin onto x_2 - x_3 projections and (c) and (d) the symmetry with respect to $x_1 = v_b$ plane onto x_1 - x_3 projections.

the transversal oscillations are absent. The other six branches correspond to four orbits: two of period-1 (called n and p) and another two of period-2 (named l_2 and m_2). To indicate the two iterations in the Poincaré section of period-2 orbits, symbols l_2^i and m_2^i , ($i = 1, 2$) are used (Fig. 3). Examining Fig. 3 in B increasing sense, it may be observed how n and p solutions are created and they later undergo two identical bifurcational processes that lead to the creation of one large chaotic attractor. Meanwhile, l_2 and m_2 coexisting solutions appear from chaotic attractors and they evolve until being destroyed. The symmetries of the system are manifested, on one hand, by the

coexistence of symmetrical solutions and, on the other hand, by the existence of symmetrical orbits with respect to itself. A first type of symmetry, corresponding to symmetrical motions of the mechanical system with respect to OXY plane (Fig. 1), is manifested by: (i) the coexistence of n and p orbits, with the mutually symmetrical projections with respect to the origin onto x_2 - x_3 coordinate plane of the phase space (Fig. 4(a)) and (ii) the l_2 and m_2 period-2 orbits, which exhibit symmetrical projections with respect to $(\pi/2, 0)$ and $(-\pi/2, 0)$ points in that same plane (Fig. 4(b)). A second type of symmetry may be observed projecting the coexisting orbits onto x_1 - x_3 coordinate

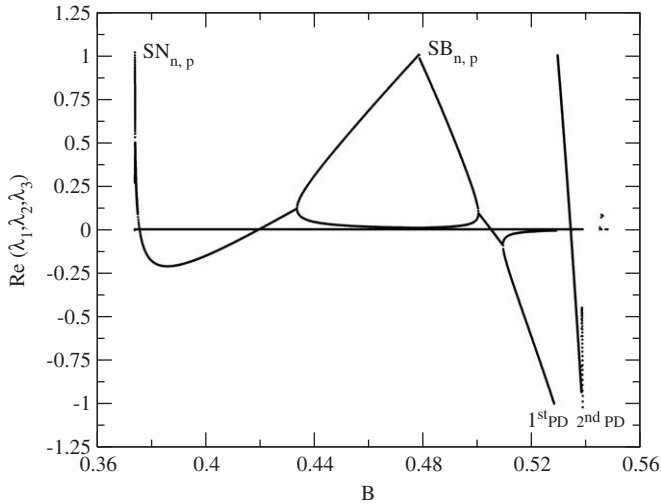


Fig. 5. The real parts of the Floquet multipliers as a function of B for n and p solutions. The values of B where the orbits become unstable are detected when one of the multipliers reaches the values 1 (saddle-nodes $SN_{n,p}$ and symmetry breaking $SB_{n,p}$) and -1 (period-doubling cascade).

plane of the phase space. After using different values of v_b parameter to compute the orbits, symmetrical projections by reflection with respect to the $x_1 = v_b$ straight line are observed. In Figs. 4(c) and (d), this type of symmetry between each (n, p) and (l_2, m_2) pairs of orbits can be seen. The existence of this symmetry indicates that the angular velocity in the transversal oscillations remains unchanged below a change of the sign of relative velocity of the O'' point (Fig. 1) with respect to the $O'X'Y'Z'$ frame. In this sense, it can be considered a *kinematic* symmetry with respect to the transversal $O'Y'Z'$ plane (see Fig. 1). With regard to the symmetry of each orbit, by examining the projections of n and p orbits (Figs. 4(a), (c)) it can be seen how these orbits are symmetrical with respect to $(\pi/2, 0)$ and $(-\pi/2, 0)$ points, respectively. On the other hand, m_2 and l_2 period-2 orbits have symmetrical x_2 - x_3 projections with respect to $(0, 0)$ and $(\pi, 0)$ points, respectively.

Orbits p and n are created by means of two saddle-node bifurcations (SN_n and SN_p in Fig. 3) situated close to the border of the chaos band. To identify these bifurcations, the Floquet multipliers were computed following p and n branches while decreasing the B parameter. At $B = 0.4$, one of the multipliers is a very small real number ($\lambda_1 \sim 10^{-6}$) and the other ones are conjugated complex numbers. As shown in Fig. 5, when B decreases the real part of complex multipliers reaches a minimum value and, immediately, it increases until $B = 0.373300\dots$, where three multipliers are lying over the real axis. Next, one of them, which is denoted as λ_2 , increases toward a value of 1 and reaching the unit circle at $B = 0.373278\dots$. Therefore, the saddle-node bifurcations SN_n and SN_p are located at this B value.

Following the evolution of p and n solutions when B is increased from $B = 0.4$, the three multipliers are real numbers beyond $B = 0.4327\dots$. Next, λ_2 increases while the other two multipliers (λ_1, λ_3) keep smaller values. At $B = 0.4776\dots$, λ_2 is crossing the unit circle (Fig. 5) and n and p orbits

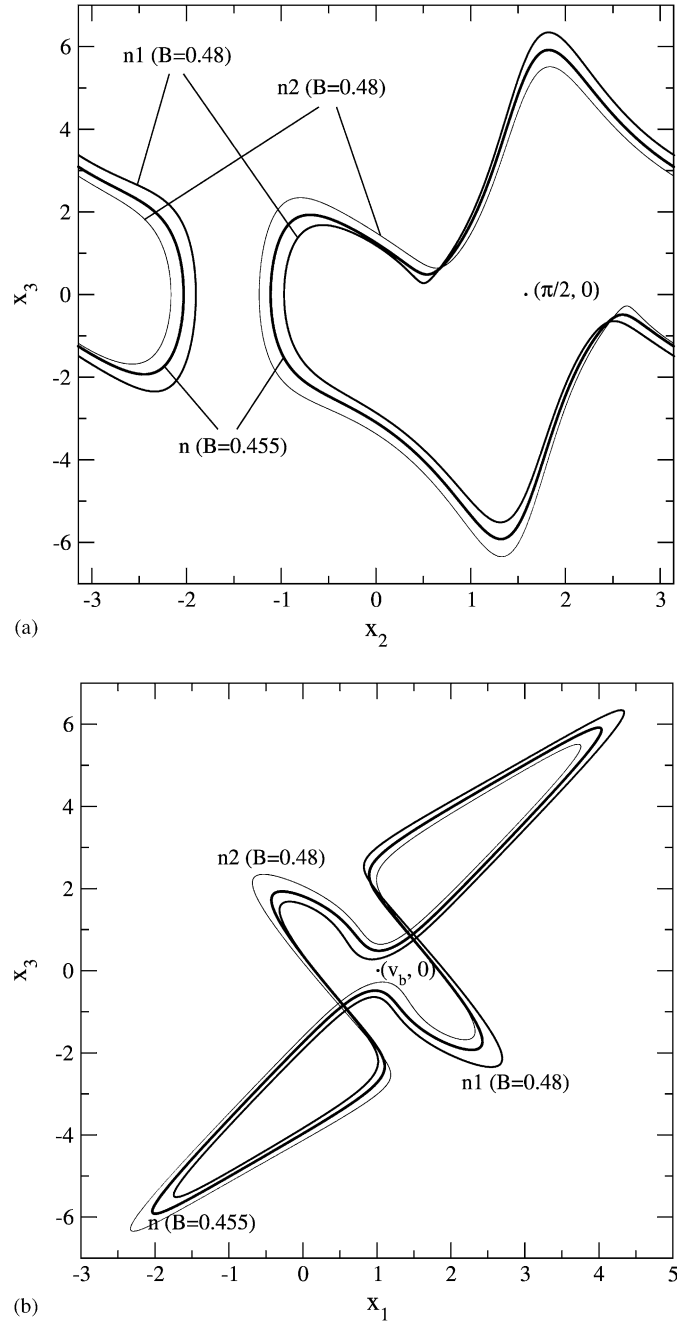


Fig. 6. Projections of trajectories illustrating the symmetry-breaking in the n orbit. At $B = 0.455$, (a) x_2 - x_3 and (b) x_1 - x_3 projections are symmetric with respect to the points $(\pi/2, 0)$ and $(v_b, 0)$, respectively. At $B = 0.48$, two $n1$ and $n2$ coexisting orbits created in the bifurcation have mutually symmetric projections with respect to both mentioned points.

become unstable via both symmetry-breaking pitchfork bifurcations (SB_n and SB_p in Fig. 3, respectively). After bifurcations, two new solutions are created in each branch ($n1$ and $n2$ from SB_n and $p1$ and $p2$ from SB_p). Numerical results show how in both simultaneous pitchfork bifurcations, the symmetry with respect to $x_1 = v_b, x_2 = \pi/2, x_3 = 0$ point is broken, and the two orbits of pairs $(n1, n2)$ and $(p1, p2)$ are mutually symmetric with respect to that point (Figs. 6(a) and (b)).

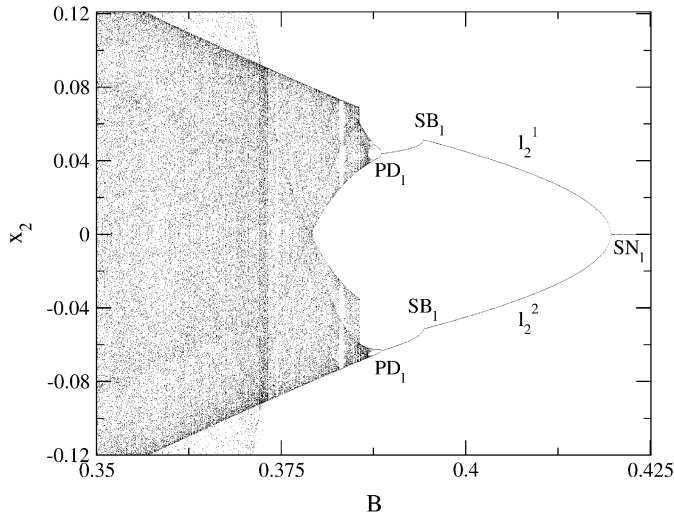


Fig. 7. Detail of bifurcation diagram showing the sequence of period-doubling (PD_1), symmetry-breaking (SB_1) and saddle-node (SN_1) bifurcations in the period-2 l_2^i ($i = 1, 2$) orbit.

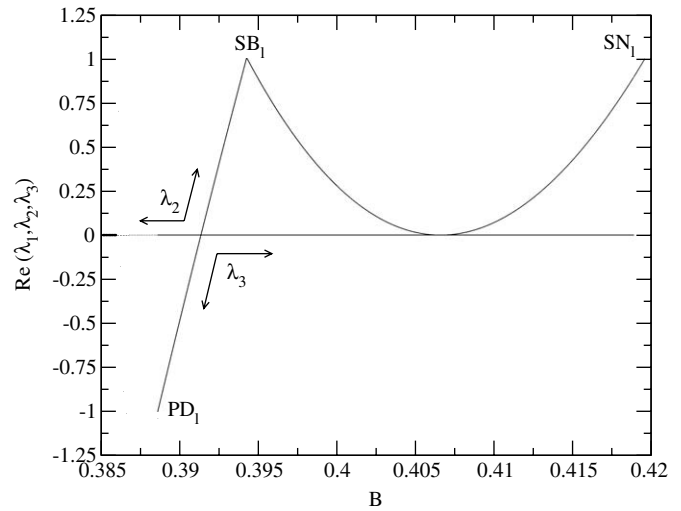


Fig. 8. Evolution of the Floquet multipliers calculated following the bifurcation diagram of the l_2^i ($i = 1, 2$) orbit (Fig. 7). At bifurcation points PD_1 , SB_1 and SN_1 , one of the multipliers is crossing the unit circle.

Following the n_1 branch, after symmetry-breaking bifurcation, the Floquet multipliers evolve as shown in Fig. 5. Thus, when B increases two multipliers are negative and one of them decreases until $B = 0.5273 \dots$, where it reaches a value of -1 . At this B value, the four solutions n_1, n_2, p_1 and p_2 become unstable, bifurcating by means of four period-doubling bifurcations, respectively, and four period-2 solutions are created. The behaviour of the dominant multiplier (λ_2) into the interval of existence of those solutions indicates that, in the bifurcation point, it lies on the unit circle ($\lambda_2 = 1$), but it immediately moves along the real axis until $B = 0.53777 \dots$, where it reaches the unit circle again, this time at the negative side ($\lambda_2 = -1$). Then, the second period-doubling bifurcation takes place in each branch. As can be seen in Fig. 3, when B continues increasing, typical cascades of period-doubling bifurcations (Feigenbaum scenario) are formed until, finally, a large chaotic attractor appears.

The two period-2 coexisting orbits l_2 and m_2 evolve identically into the same interval of existence. In Figs. 7 and 8, x_2 - B bifurcation diagram and the evolution of the Floquet multipliers corresponding to the l_2 orbit are shown, respectively. When B increases a bifurcational sequence inverse to that displayed in the evolution of n and p orbits is observed. Thus, at $B = 0.388611 \dots$, one of the multipliers (λ_3) is lying over the unit circle in the negative side of the real axis indicating a period-doubling bifurcation (PD_1 in Fig. 8), while the other two multipliers are very small real numbers ($\lambda_1, \lambda_2 \sim 10^{-9}$). When B increases, $|\lambda_3|$ decreases until it reaches values in the range of 10^{-9} . At this point, λ_2 begins to increase quickly until at $B = 0.394290 \dots$, it crosses the unit circle at the positive side of the real axis. In this way, a symmetry-breaking bifurcation (SB_1) takes place. Finally, as it is shown in Fig. 8, λ_2 evolves until it reaches again the value 1 (saddle-node bifurcation SN_1) at $B = 0.41956 \dots$, and then, the orbit is destroyed.

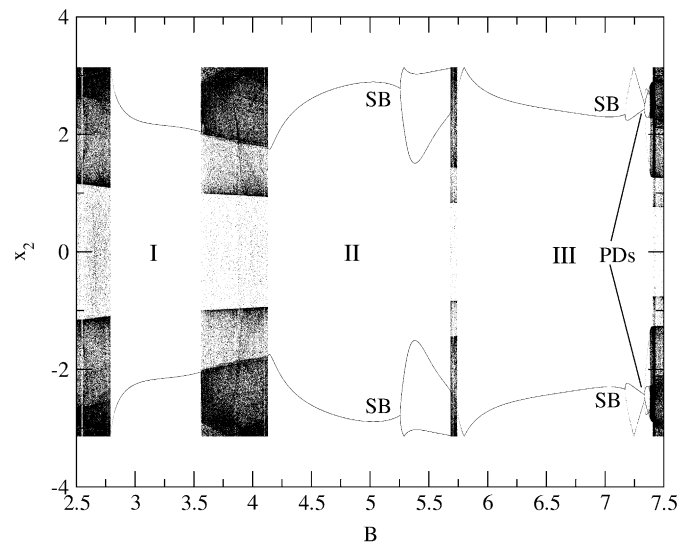


Fig. 9. Bifurcation diagram showing three consecutive intervals of periodicity, alternating with chaotic band, where the system exhibits: (I) only intermittent transitions to chaos; (II) intermittency, symmetry-breaking and intermittency, and (III) intermittency, symmetry-breaking and period-doubling cascade to chaos.

4.2. Mean-large forcing amplitudes

At $B \gtrsim 1.75$ the system exhibits several types of periodic behaviours which evolve in different ways. Thus, in Fig. 9 three successive intervals (labelled as I, II and III) are shown, where periodic solutions behave of three distinct way when the control parameter is varied. In spite of the existence of different dynamics, the three intervals have one common characteristic: orbits undergo intermittent transitions on the left limit of periodic intervals. To exemplify this phenomenon the attention will be focused on the interval III of Fig. 9. Starting

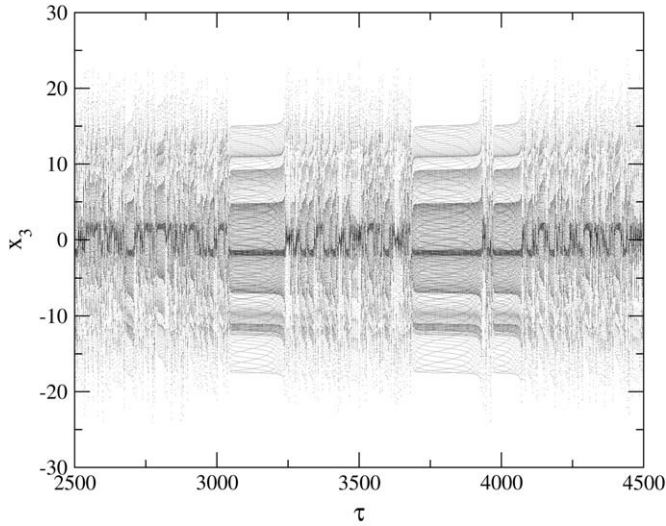


Fig. 10. Time series of the variable x_3 calculated at $B = 5.739000\dots$, near intermittent transition. Chaotic bursts alternating with laminar phases are shown.

from $B > 5.739080\dots$, after a chaotic band, two branches, corresponding to two coexisting period-1 orbits, can be clearly distinguished. When B decreases from the lower limit ($B = 5.739050\dots$) of the periodic interval, two coexisting orbits are destroyed by both saddle-node bifurcations, taking place an intermittent transition of type I [12]. The numerical results, at $B = 5.739000\dots$, close to the limit of chaos band, show the typical behaviour described in the literature [9,13]. Thus, a set of successive iterations of Poincaré map are visiting small phase-space regions where the destroyed periodic solutions were situated (laminar phase). The attractor spends a variable stretch of time there, and after this, the iterations suddenly burst out and go over the large chaotic attractor formed after the two simultaneous bifurcations. Finally, the iterations return to the old periodic attractor region and the process is repeated again and again. In Fig. 10, the dynamics described above is shown through the behaviour of x_3 - τ time series. Following the evolution of solutions into the interval III, increasing B values, it is observed how they behave in the same way as n and p orbits, i.e. symmetry-breaking bifurcations and period-doubling cascades take place before a large chaotic attractor appears.

In the lower limit of the interval II of Fig. 9, two coexisting period-1 solutions are created in both intermittency transitions. Fig. 11 shows the evolution of Floquet multipliers in this interval. In the neighbourhood of the left limit of the interval, the three Floquet multipliers are real numbers and, when B decreases, one of them increases very quickly toward 1, indicating the proximity of the saddle-node bifurcation associated to type I intermittency [9]. Next, a symmetry-breaking pitchfork bifurcation can be detected in each branch at $B = 5.259\dots$. After these bifurcations, one of the multipliers (λ_3) moves along the negative part of the real axis toward the unit circle, predicting a period-doubling bifurcation as happened in n and p branches (Fig. 5), and also in solutions into the interval III. Nevertheless, the situation changes with respect to these cases, since λ_3

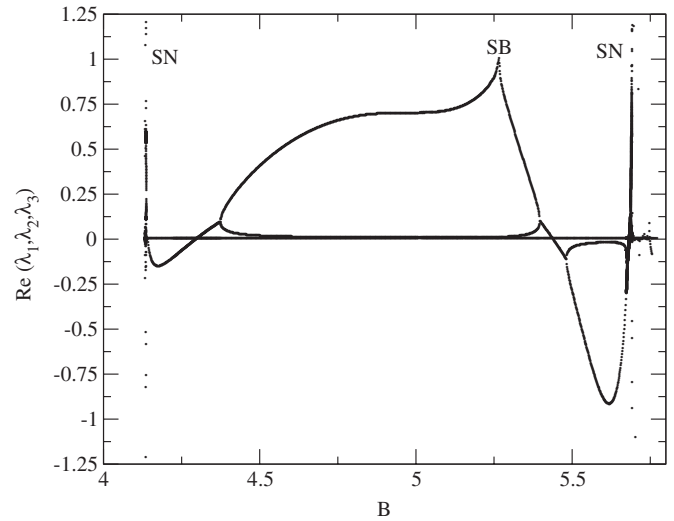


Fig. 11. Evolution of the Floquet multipliers calculated following the bifurcation diagram into the interval II (Fig. 9). After symmetry-breaking one multiplier decreases toward the value -1 , but returns without reaching the unit circle and the period-doubling bifurcation does not occur. Two saddle-node bifurcations associated to both intermittent transitions to chaos are detected at the limits of the interval.

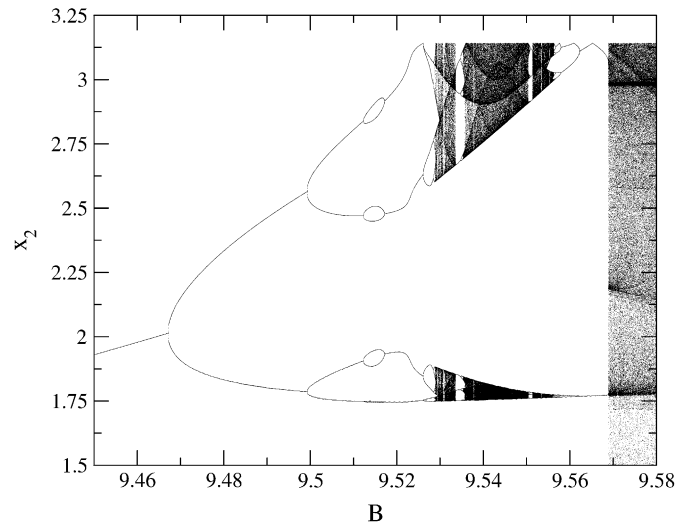


Fig. 12. Magnification of one of the branches of the bifurcation diagram showing, at large B values, a complex bifurcational behaviour, previous to the creation of a large chaotic attractor.

multiplier approaches the unit circle until reaching the minimum value $\lambda_3 = -0.9175\dots$ at $B = 5.611\dots$, without reaching the value -1 . Thus, when B increases, it returns immediately toward high values and the period-doubling bifurcation does not occur, as usually happens after symmetry-breaking bifurcation. If the Floquet multipliers are interpreted as indicators of the stability of the orbits, then the fact observed can be described as the tendency of the system to lose the stability after symmetry-breaking. However, as can be seen, the sequence: symmetry-breaking, period-doubling cascade and chaos does not always occur. In this case, as happened in the lower limit

of the interval, the dynamics of the system turns chaotic in the upper limit of the interval through intermittent transitions of type I. In Fig. 11, it can be seen how the behaviour of Floquet multipliers is the same in the neighbourhood of both limits of the interval II. Into the preceding interval (called I), a relatively simple behaviour can be observed. Thus, two period-1 coexisting orbits evolve without any bifurcation taking place between the two successive intermittent transitions, where the orbits are created and destroyed, respectively.

At larger B values, the evolution of periodic attractors usually follows the pattern: intermittent transition, symmetry-breaking and period-doubling cascade to chaos. Nevertheless, different and more complicated behaviours can be found in the route to the formation of the large chaotic attractor located between two successive periodic intervals. For instance, in Fig. 12 it is seen how, when B increases, typical cascades are not produced, and when period-8 orbits have been created after the third period-doubling bifurcations, the solutions return again to be four-periodic through reverse period-doubling bifurcations. From

these solutions, typical period-doubling cascades lead to the creation of two small coexisting chaotic attractors. When B continues to increase, reverse period-doubling sequences create coexisting period-2 orbits, which undergo intermittent transitions and, thus, give rise to the formation a large chaotic attractor.

5. Collection of chaotic attractors

As it was seen in the overview of bifurcation diagrams shown in Fig. 2, large chaotic attractors are systematically appearing when the B control parameter is varied. To obtain a qualitative information about changes undergone in the chaotic dynamics, a large number of attractors were calculated, and to get clearer three-dimensional pictures, the variable $x_2 \in [-\pi, \pi]$ had been transformed to $x'_2 \in [0, 2\pi]$. In the following some of these attractors are described.

At lower B values, the structure of chaotic attractors is characterized by tight stripes spreading in the $(0, 2\pi)$ interval of the x'_2 variable (Fig. 13(a)), and changing into loops in the

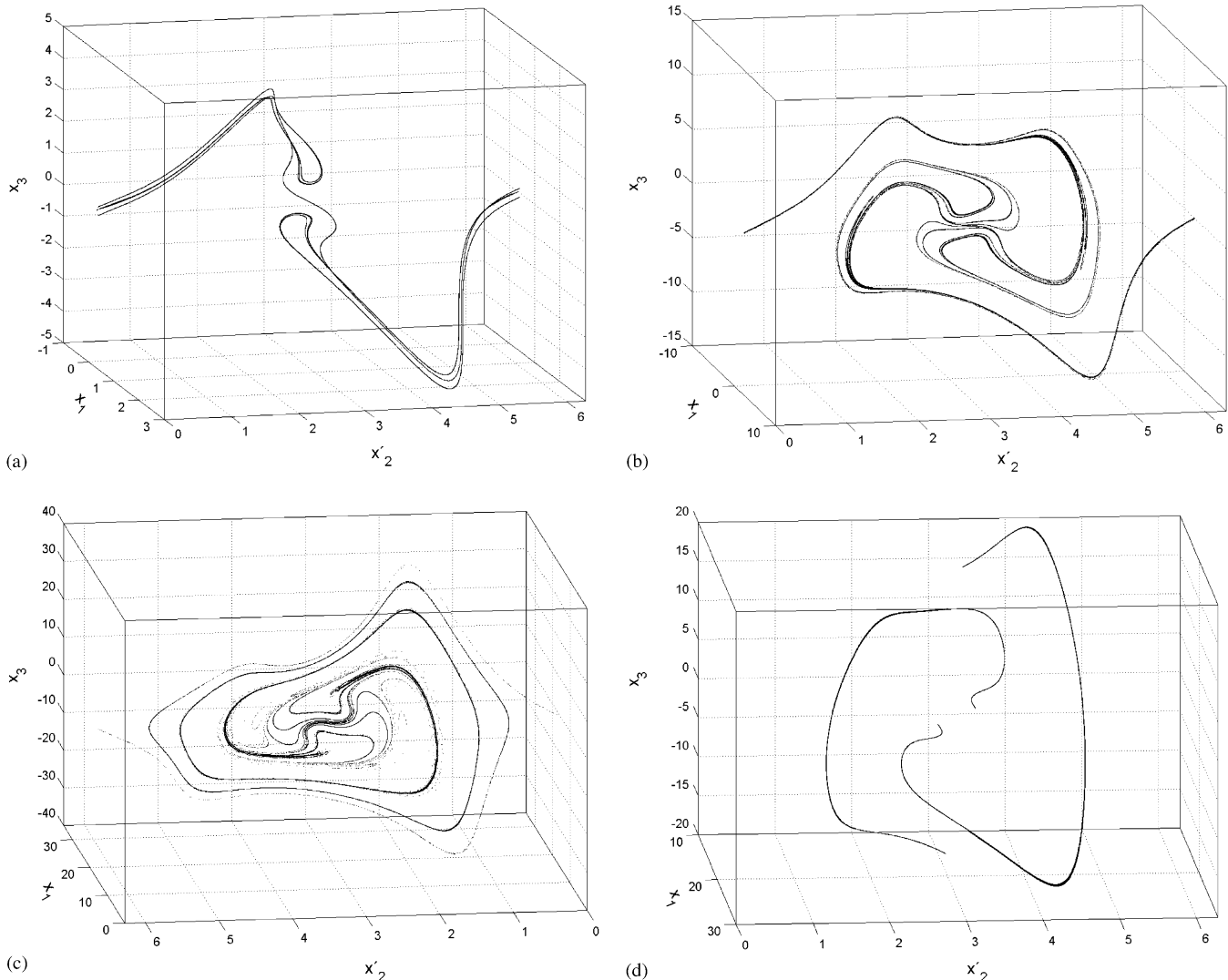


Fig. 13. Collection of chaotic attractors showing, at first, an increase in the structure complexity: (a) $B = 0.2$, (b) $B = 1.5$ and (c) $B = 9.58$, and later, (d) the coexistence chaos–chaos of two simple attractors ($B = 12$).

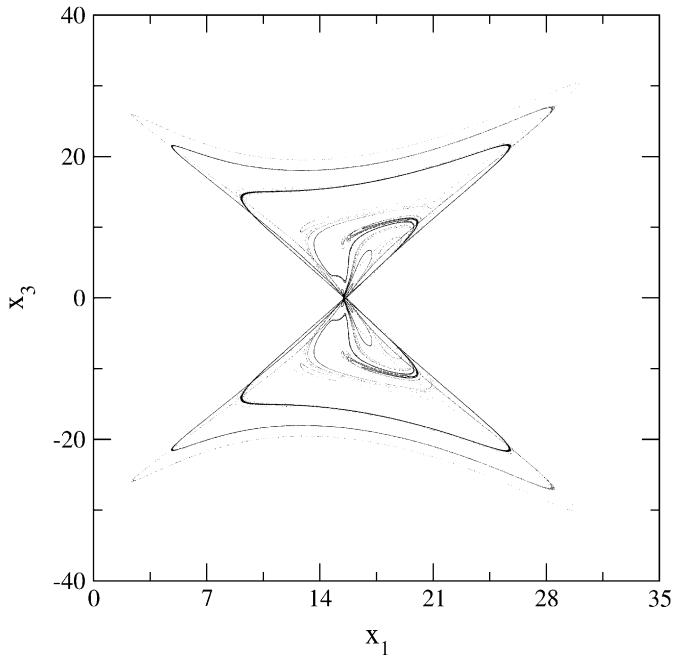


Fig. 14. Projection of the chaotic attractor at $B=9.58$ onto x_1 – x_3 coordinate plane.

neighbourhood of $(x_1, x_2', x_3) \equiv (0, \pi, 0)$ phase-space point. As B increases, the dynamics of the attractors corresponding to the successive chaotic bands undergoes a continuous evolution characterized by an increasingly more complicated dynamics centred on the $(0, \pi, 0)$ point (Fig. 13(b)). As a result, the points situated in the neighbourhood of the $x_2' = 0$ plane are rarely visited. This process is maintained until the chaotic band situated into $B \in (9.568 \dots, 9.771 \dots)$ interval, where big attractors exist (Fig. 13(c)). After the following periodic interval, the chaotic dynamics changes drastically and, at $B \gtrsim 11.913 \dots$, the complex structure of the attractors of the preceding chaotic bands disappears, and is replaced by simple structures where the attractors acquire the shape of thin stripes. Nevertheless, in this new situation, two chaotic attractors are coexisting and, therefore, it can be established that, at large forcing amplitudes, the chaotic behaviour of the system is characterized by coexistence chaos–chaos. As an example, two coexisting chaotic attractors calculated for $B = 12$ are shown (Fig. 13(d)).

Symmetries of the three-dimensional chaotic attractors are revealed by analysing the projections onto the coordinate planes. Thus, the characteristics symmetries with respect to the origin and x_3 -axis (reflection) are, respectively, observed in x_2 – x_3 and x_1 – x_3 projections (Fig. 14). Likewise, symmetry by reflection with respect to x_1 -axis may be observed in x_1 – x_3 plane.

6. Basins of attraction

As usual in many dynamical systems, phase space of the system studied is arranged by the coexistence of two or more attractors, since each collection of initial conditions whose

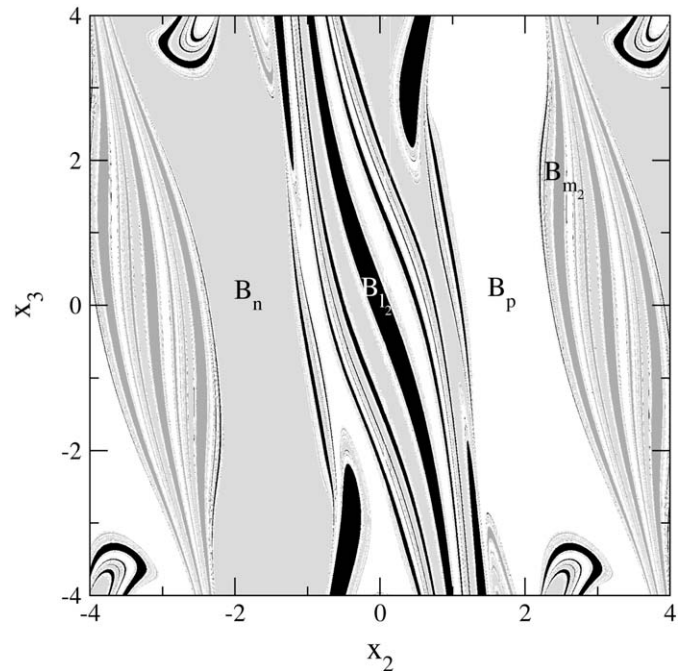


Fig. 15. Cross section at $x_1 = 0$ plane of the basins of attraction computed at $B = 0.4$. The basins B_n (grey), B_p (white), B_{l_2} (black) and B_{m_2} (dark grey) corresponding to four coexisting orbits are shown.

trajectories go to one determined attractor defines a set of points (basin of attraction) associated to that attractor. The structure of phase space induced by the basins of attraction may become complicated when several basins exist, and moreover, when the boundaries between them are fractal structures [14,15] instead of smooth curves. In this case, basins of attraction were computed by exhaustively solving the dynamical system using initial conditions on a 1255×1255 grid, and fractal boundaries were found throughout.

In Fig. 15 a cross section ($x_1 = 0$ plane) of the three-dimensional phase space is shown, at $B = 0.4$. Four basins found: B_n (light grey), B_p (white), B_{l_2} (black) and B_{m_2} (dark grey) corresponding, respectively, to the four-periodic attractors coexisting at that value of the B parameter. It can be seen how the arrangement of the basins exhibits the characteristic symmetry of the system with respect to the origin of coordinates and with respect to the $(0, \pm\pi, 0)$ point. On the other hand, the fractal structure of the boundaries of the basins is clearly observed. When a small zone of the basin is again computed using higher resolution (Fig. 16), an examination of the fractal boundaries indicates that they are formed by points belonging to the four basins of attraction. Following Kennedy and Yorke [16], it can be established that *each point that is on the boundary of one region is on the boundary of all (Wada property)*, and therefore, the boundaries of the basins in Fig. 15 are *Wada basin boundaries*. This indicates that initial conditions in the neighbourhood of boundaries produce a dynamical behaviour difficult to predict [17], since the system can be conducted to any of the four coexisting orbits.

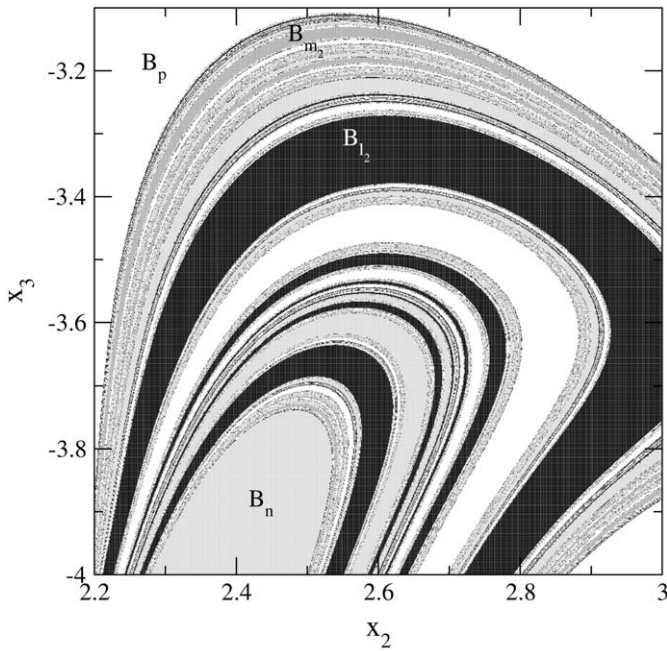


Fig. 16. Detail of Fig. 15, where the Wada basin boundaries can be clearly seen.

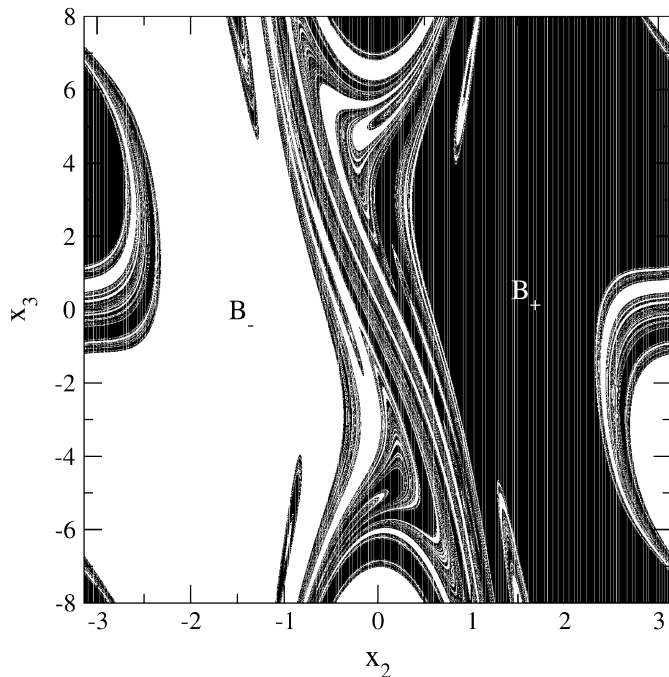


Fig. 17. Basins of attraction belonging to two coexisting period-1 orbits into the interval I (Fig. 9). Fractal structures can be observed in spite of the simplicity of the dynamics in that interval.

It had been shown that, at mean-large B values, periodic intervals exist where only two solutions are coexisting and where the bifurcation scenario is relatively simple in comparison with the situation observed at low B values. Nevertheless, the structure of the phase space does not evolve to become simpler in the

sense of observing big basins with smooth boundaries. Thus, Fig. 17 shows the two basins (at $x_1 = 0$ plane) B_+ and B_- , calculated for $B = 3$, into the interval called I . These basins of attraction correspond, respectively, to both coexisting orbits ($x_2 > 0$ and $x_2 < 0$) which evolve without any bifurcation, except intermittent transitions to chaos. In this case, basins are formed by a great amount of pieces with fractal boundaries between them. This structure becomes more pronounced around $x_2 = 0$ and $x_2 = \pi$ planes, as happened in the basins computed for $B = 0.4$ (see Fig. 15). Therefore, it seems that the fractality and a characteristic arrangement of the basins constitute a hallmark of the system, independently the quantity of coexisting solutions.

7. Summary

We have presented a numerical study of three-dimensional dynamical system obtained from the mechanical problem concerning a sliding rigid body, periodically forced and subjected to dry friction. This system, which can be considered a simple model of a sliding device or an articulated sliding vehicle undergoing lateral oscillations, has a varied periodic and chaotic dynamics which is very sensitive to the forcing amplitude values. It was found that the system behaves according to a pattern characterized by alternating periodic and chaotic states. Diverse bifurcational episodes were detected when the system evolves by variation of forcing amplitude values. Thus, sequence of bifurcations: saddle-node, symmetry-breaking and period-doubling (cascades) are typically found at low forcing amplitude values. In other cases, it may be observed sequences formed by intermittent transition to chaos and symmetry-breaking bifurcation accompanied either by other intermittent transition to chaos or Feigenbaum route to chaos (period-doubling cascade). Likewise, more complex sequences were found. The bifurcations have been characterized by systematic calculations of the Floquet multipliers when the dynamics of the system changes. In this respect, we can remark that the Floquet multipliers evolve into different intervals of periodicity following a characteristic pattern (see, Figs. 5 and 11).

The evolution of the chaotic behaviour of the system has been described, after calculating a collection of chaotic attractors varying the value of the forcing amplitude. Certain regularity has been found in the appearance of the chaotic motion, and also in how the attractors become tangled when the control parameter increases. Another interesting aspect is the sudden change observed in the chaotic motion when the forcing amplitude reaches a certain value, after which, the attractors take the shape of tight pieces and the coexistence chaos–chaos appears.

Finally, the basins of attraction computed for several control parameter values exhibit, as a general rule, layered fractal structures in their boundaries. At low forcing amplitude values, where more than two solutions are coexisting, fractal layered structures are Wada basin boundaries, which can produce a certain unpredictability to know the final output of the system. At mean values of the control parameter, the fractality is maintained and again fractal structures can be observed in basin boundaries.

Acknowledgements

Authors wish to thank Dr. Dominguez de la Vega for his generous help in the revision of this paper and for his useful comments and advices.

References

- [1] B. Blazejczyk-Okolewska, K. Czołczynski, T. Kapitaniak, J. Wojewoda, *Chaotic Mechanics in Systems with Impacts and Friction*, World Scientific, Singapore, 1999.
- [2] B. Feeny, A. Guran, N. Henrichs, K. Popp, A historical review on dry friction and stick-slip phenomena, *Appl. Mech. Rev.* 51 (1998) 321–341.
- [3] R. Ibrahim, Friction induced vibration, chatter, squeal and chaos Part I: dynamics and modelling, *Appl. Mech. Rev.* 47 (1994) 227–253.
- [4] E.J. Berger, Friction modelling for dynamic system simulation, *Appl. Mech. Rev.* 55 (2002) 535–578.
- [5] M.A. Heckl, I.D. Abrahams, Active control of friction-driven oscillations, *J. Sound Vib.* 193 (1996) 417–426.
- [6] Y.F. Lim, K. Chen, Dynamics of dry friction: a numerical investigation, *Phys. Rev. E* 58 (5) (1998) 5637–5642.
- [7] P. Vielsack, Stick-slip instability of decelerative sliding, *Int. J. Non-Linear Mech.* 36 (2001) 237–247.
- [8] Y. Ueda, Survey of regular and chaotic phenomena in the forced Duffing oscillator, *Chaos Solitons Fractals* 1 (1991) 191–231.
- [9] A.H. Nayfeh, B. Balachandran, *Applied Nonlinear Dynamics. Analytical, Computational, and Experimental Methods*, Wiley, New York, 1995.
- [10] Y.A. Kuznetsov, *Elements of Applied Bifurcation Theory*, Springer, New York, 1998.
- [11] J.M.T. Thompson, H.B. Stewart, Y. Ueda, Safe, explosive, and dangerous bifurcations in dissipative dynamical system, *Phys. Rev. E* 49 (1994) 1019–1027.
- [12] Y. Pomeau, P. Manneville, Intermittent transition to turbulence in dissipative dynamical system, *Commun. Math. Phys.* 74 (1980) 189–197.
- [13] J.M.T. Thompson, H.B. Stewart, *Nonlinear Dynamics and Chaos*, Wiley, Chichester, 1997.
- [14] S.W. McDonald, C. Grebogi, E. Ott, J.A. Yorke, Fractal basin boundaries, *Physica D* 17 (1985) 125–153.
- [15] E. Ott, *Chaos in Dynamical Systems*, Cambridge University Press, Cambridge, 2002.
- [16] J. Kennedy, J.A. Yorke, Basins of Wada, *Physica D* 51 (1991) 213–225.
- [17] J. Aguirre, M.A.F. Sanjuán, Unpredictable behavior in the Duffing oscillator: Wada basins, *Physica D* 171 (2002) 41–51.